HEALTH AND MEDICINE

Enhancing the regenerative effectiveness of growth factors by local inhibition of interleukin-1 receptor signaling

Ziad Julier[1]*, Rezvan Karami[1]*, Bhavana Nayer[1], Yen-Zhen Lu[1], Anthony J. Park[1], Kenta Maruyama[2], Gisela A. Kuhn[3], Ralph Müller[3], Shizuo Akira[2], Mikaël M. Martino[1,2†]

Although growth factors (GFs) are key molecules for regenerative medicine, their use has been limited by issues associated with suboptimal delivery systems and incomplete understanding of their signaling dynamics. Here, we explored how proinflammatory signals affect GF regenerative potential. Using bone regeneration in mouse, we found that the regenerative capacity of two clinically relevant GFs (BMP-2 and PDGF-BB) is impaired by interleukin-1 receptor (IL-1R1). Mechanistically, IL-1R1 activation in bone-forming cells desensitizes them to GFs and accelerates senescence. Moreover, administration of the GFs triggers IL-1 release by macrophages. To provide localized and sustained IL-1R1 inhibition, we engineered IL-1R antagonist (IL-1Ra) to bind the extracellular matrix (ECM) very strongly and demonstrate that codelivering GFs with ECM-binding IL-1Ra induces superior regeneration. Thus, we highlight that GF regenerative activity is hindered by proinflammatory signals, and GF-based therapies should integrate immunomodulation. Particularly, ECM-binding IL-1Ra holds clinical translational potential by enhancing efficacy of GF therapies.

INTRODUCTION

Growth factors are powerful molecules capable of stimulating a variety of cellular processes including cell proliferation, migration, and differentiation. Therefore, they have raised a lot of hope for regenerative medicine, and several growth factor–based products have reached clinical applications (*1*). Nevertheless, therapies based on recombinant growth factors are still hindered by limitations that include ineffectiveness at low doses and serious side effects at high doses (*2*, *3*). For example, these limitations have led the U.S. Food and Drug Administration (USFDA) to release boxed warning for some growth factors such as bone morphogenetic protein-2 (BMP-2) and platelet-derived growth factor–BB (PDGF-BB) (*2*, *3*). The issues that limit growth factors in regenerative medicine are certainly linked to the use of suboptimal delivery systems. Thus, various strategies have been developed to ensure precise localization of recombinant growth factors in tissues and control their release (*4*). However, controlling growth factor localization and release may just be the first step to improve their regenerative potential and safety. Understanding how the signaling of growth factors is affected by the tissue microenvironment once they are released is likely of utmost importance. An immune response almost always accompanies the tissue repair regeneration processes (*5*, *6*), but the impact of the immune system and inflammatory signals on growth factor signaling has been overlooked and is poorly understood. In particular, the response of cells to growth factors could change depending on the inflammatory and immune microenvironment at the delivery site (*6*). Moreover, although growth factors are delivered with the hope of targeting cells that make new tissues such as tissue-resident stem cells and progenitor cells, they would inevitably also act on immune cells present in damaged tissues, as many of them express growth factor receptors (*7*, *8*). However, the response of immune cells following a local delivery of recombinant growth factors is still elusive.

The proinflammatory cytokine interleukin-1 (IL-1) and its ubiquitously expressed receptor (IL-1R1) are central mediators of innate immunity and inflammation, virtually affecting all cells and organs (*9*). Moreover, IL-1R1 has been shown to have a significant impact in the repair and regeneration of various tissues (*5*, *10*). For example, we found that IL-1R1 activation inhibits the bone regenerative activity of compact bone–derived mesenchymal stromal cells (called MSCs herein) (*10*). On the basis of these findings, we developed a cell delivery system that integrates an inhibitor of MyD88, which is an adaptor protein critical in the IL-1R1 signaling pathway. Here, we investigated the extent to which IL-1R1–mediated proinflammatory signaling affects tissue regeneration driven by recombinant growth factors, with the ultimate goal of designing successful regenerative strategies that integrate control of the immune system. As a model system, we used bone regeneration in mice driven by BMP-2 and PDGF-BB, which are two clinically relevant growth factors for regenerative medicine.

RESULTS

Enhanced regenerative effect of BMP-2 and PDGF-BB in *Il1r1*$^{-/-}$ mice

To evaluate the importance of IL-1R1 during bone regeneration driven by local delivery of growth factors, we first analyzed the regenerative capacity of recombinant BMP-2 and PDGF-BB in an IL-1R1 knockout mouse. As a typical bone regeneration model, we used critical-size calvarial defects that we treated with the growth factors delivered via a fibrin matrix. Two months after treatment, the coverage of the defects with mineralized bone as well as the volume of new bone formed was measured. As expected, delivering BMP-2 and PDGF-BB in wild-type mice enhanced regeneration to some extent. However, the regenerative effect of both growth factors was significantly enhanced in *Il1r1*$^{-/-}$ mice, suggesting that IL-1R1 signaling impairs regeneration driven by BMP-2 and PDGF-BB (Fig. 1).

[1]European Molecular Biology Laboratory Australia, Australian Regenerative Medicine Institute, Monash University, Melbourne, VIC, Australia. [2]Laboratory of Host Defense, World Premier Institute Immunology Frontier Research Center, Osaka University, Osaka, Japan. [3]Institute for Biomechanics, ETH Zurich, Zurich, Switzerland.
*These authors contributed equally to this work.
†Corresponding author. Email: mikael.martino@monash.edu

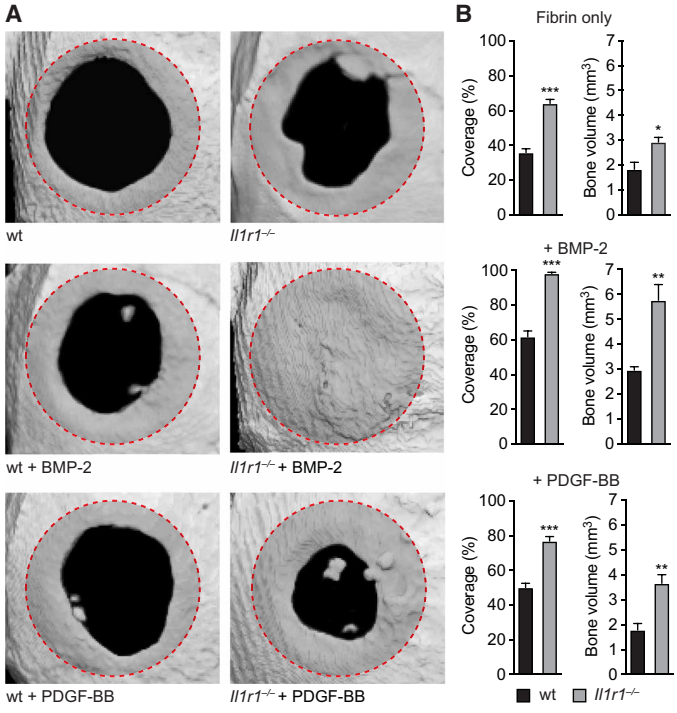

Fig. 1. Bone regeneration driven by BMP-2 and PDGF-BB is enhanced in *Il1r1*$^{-/-}$ mice. (**A** and **B**) Critical-size calvarial defects (4.5-mm diameter) in wild-type (wt) or *Il1r1*$^{-/-}$ mice were treated with BMP-2 or PDGF-BB (1 μg) delivered by a fibrin matrix. Eight weeks after treatment, bone regeneration was measured by micro–computed tomography (microCT). Representative calvarial reconstructions (average of the individual samples) are shown in (A). Original defect area is shaded with a dashed outline. Coverage of defects and volume of new bone formed are shown in (B). Data are means ± SEM. $n = 6$. Student's t test. $^{**}P < 0.01$; $^{***}P < 0.001$.

Inhibition of the response of bone-forming cells to growth factors by IL-1R1 signaling

During bone regeneration, BMP-2 induces differentiation of bone-forming cells, i.e., skeletal stem/progenitor cells and osteoblasts, while PDGF-BB induces both migration and proliferation of these cells (*2*). Thus, we examined whether IL-1β—the main IL-1R1 ligand released following bone injury (*10*)—affects the ability of growth factors to induce these key cellular processes. As for bone-forming cell models, we used MSCs (fig. S1) and osteoblasts. IL-1β significantly inhibited the capacity of BMP-2 to up-regulate osteoblast-specific genes and to induce matrix mineralization in MSCs (Fig. 2, A and B). The same inhibitory effect was observed with the expression of differentiation markers in osteoblasts (fig. S2A). Since MSCs highly express PDGF receptor β (PDGFRβ or CD140b; fig. S1), their stimulation with PDGF-BB enhances colony-forming unit fibroblasts (CFU-F) formation. However, we found that IL-1β inhibits the boosting effect of PDGF-BB on CFU-F formation (Fig. 2, C and D). Similarly, IL-1β inhibited PDGF-BB–driven MSC and osteoblast proliferation and migration (Fig. 2, E and F, and fig. S2, B and C), further supporting that IL-1R1 signaling impairs the response of these bone-forming cells to growth factors. Last, the inhibitory effect of IL-1β was not observed in *Il1r1*$^{-/-}$ MSCs, confirming that the cytokine inhibits the response of the cells to BMP-2 and PDGF-BB via IL-1R1 (fig. S3).

Desensitization to growth factors in MSCs and osteoblasts exposed to IL-1R1 signaling

We explored whether IL-1R1 activation affects Smad proteins, because they are critical in BMP-2 signaling transduction (*11*). We found that Smad1 phosphorylation in response to BMP-2 is significantly lower, when MSCs and osteoblasts are prestimulated with IL-1β (Fig. 3A and fig. S4A). In addition, stimulation of MSCs and osteoblasts with IL-1β leads to a decrease of total Smad1/5/8 proteins (Fig. 3B and fig. S4B). IL-1β significantly up-regulated the expression of the E3 ubiquitin-protein ligase Smurf2 (Fig. 3, C and D), which targets Smad1/5/8 for ubiquitination and degradation (*12*). Thus, to validate that IL-1β inhibits BMP-2–driven osteoblastic differentiation via Smad1/5/8 degradation by Smurf2, we used heclin, a selective inhibitor of Smurf2 (*13*). Inhibition of BMP-2–driven osteoblastic differentiation by IL-1β was stopped in the presence of heclin as shown by a rescue of matrix mineralization (Fig. 3E). Further confirming the IL-1β–Smurf2–Smad1/5/8 axis, Smad1/5/8 degradation following IL-1β stimulation was inhibited in the presence of heclin (Fig. 3F).

Since Akt (protein kinase B) phosphorylation is central in PDGF-BB signaling (*14*), we tested whether IL-1R1 stimulation affects this kinase. When MSCs and osteoblasts were preincubated with IL-1β, Akt phosphorylation, which is normally induced after PDGF-BB stimulation, was rapidly turned down (at Ser_{473}) (Fig. 3G and fig. S4C), indicating that Akt dephosphorylation is faster when cells are exposed to IL-1R1 signaling. Because Akt dephosphorylation is mainly driven by pleckstrin homology domain leucine-rich repeat protein phosphatases (PHLPPs) (*14*), we further tested whether IL-1β modulates their expression. We found that MSC stimulation with IL-1β quickly increases the expression of PHLPPs (Fig. 3, H and I). Then, to verify that IL-1β inhibits the response to PDGF-BB via PHLPP-driven dephosphorylation of Akt, we used NCS-45586, which is a selective inhibitor of PHLPPs (*15*). Inhibition of MSC proliferation and migration by IL-1β as well as Akt dephosphorylation were suppressed in the presence of NCS-45586 (Fig. 3, J to L), confirming the IL-1β–PHLPPs–Akt pathway. Last, we tested whether IL-1R1 signaling affects the cell responsiveness to the growth factors by changing the expression of their receptors. Treatment of MSCs with IL-1β had no significant effect on BMP-2 and PDGF-BB receptor cell surface expression (fig. S5).

Next, we also explored the effect of IL-1R1 activation on MSC senescence, because Smurf2 has been linked to this cellular process (*16*–*18*). We chose to measure senescence-associated β-galactosidase (SA-β-gal), as an increase of its activity is considered a hallmark for senescence (*19*). We found that treatment of MSCs with IL-1β increases SA-β-gal activity in a time-dependent manner, suggesting that IL-1β accelerates the induction of senescence in these cells (Fig. 3, M and N). In addition, MSC treatment with IL-1β induced the secretion of typical senescence-associated cytokines including IL-6, CC chemokine ligands 1 (CCL1) and 3 (CCL3), and CXC chemokine ligand 1 (CXCL1; IL-8 homolog in the mouse) (fig. S6).

Induction of IL-1β release by macrophages following local delivery of BMP-2 or PDGF-BB

Because IL-1β is the main IL-1R1 ligand in the context of bone healing (*10*), we measured its concentration in calvarial defects following treatment with growth factors. Unexpectedly, while IL-1β was released after bone injury, delivering BMP-2 or PDGF-BB led to a significant increase of the cytokine during the first 2 weeks following

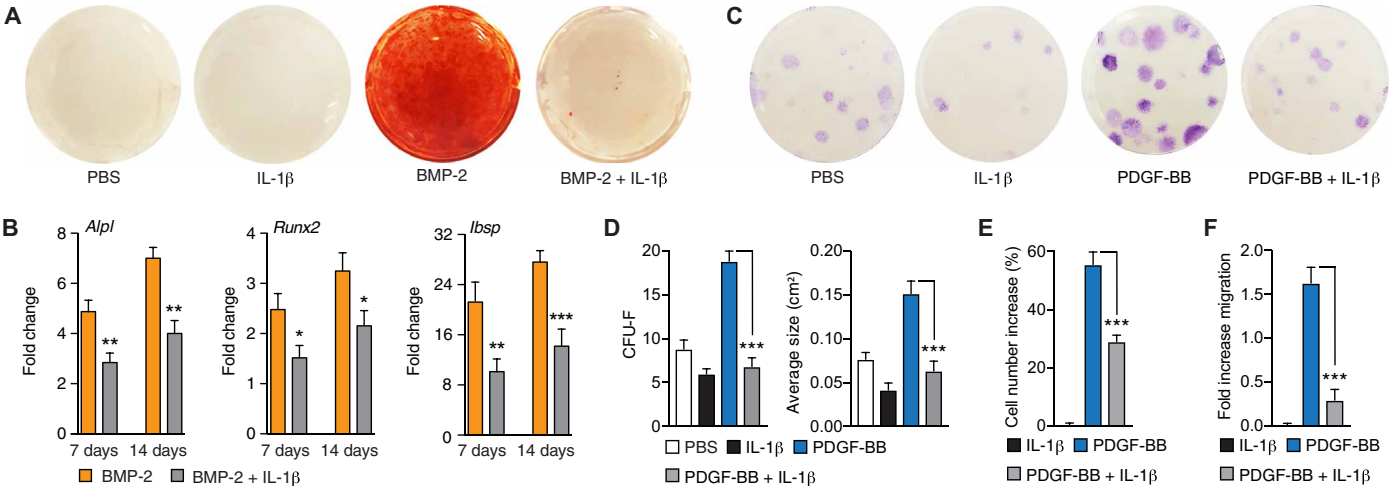

Fig. 2. IL-1β inhibits the morphogenic activity of BMP-2 and PDGF-BB. (**A** and **B**) MSCs were cultured in normal medium or osteogenesis induction medium containing BMP-2 and IL-1β. Matrix mineralization was detected with alizarin red after 21 days. Representative wells (2 cm^2) are shown in (A). Expression of osteoblast-specific genes was determined by quantitative polymerase chain reaction (PCR). Fold changes in gene expression relative to MSCs cultured in normal medium are shown in (B). *Alpl*, alkaline phosphatase; *Runx2*, runt-related transcription factor 2; *Ibsp*, integrin-binding sialoprotein. $n = 4$. (**C** and **D**) MSCs were seeded for 10 days with PDGF-BB and IL-1β. Representative wells (9 cm^2) are shown in (C). Graphs in (D) show CFU-F and average size of colonies. $n = 6$. (**E**) MSC proliferation in response to PDGF-BB and IL-1β after 72 hours. $n = 6$. (**F**) MSC Transwell migration induced by PDGF-BB and IL-1β (increase over basal migration after 6 hours). $n = 6$. For all panels, data are means ± SEM. For (B), Student's *t* test. For (D) to (F), one-way ANOVA with Bonferroni post hoc test. $^*P < 0.05$; $^{**}P < 0.01$; $^{***}P < 0.001$.

treatment (Fig. 4A). Next, to determine which cell type was the primary source of IL-1β in the defect microenvironment, we repeated the experiment in mice where macrophages were depleted by clodronate liposomes (fig. S7), since these cells release large amounts of IL-1β (*20*). In the absence of macrophages, IL-1β concentration in the bone defects was not enhanced by the delivery of BMP-2 or PDGF-BB, suggesting that the two growth factors trigger the release of IL-1β via macrophages (Fig. 4B). We confirmed that primary bone marrow–derived macrophages (unpolarized) are equipped to respond to PDGF-BB and BMP-2 since they express some of their receptors (PDGFRα, PDGFRβ, and activin receptor type-1 (ACVR1) as well as BMP receptor type-1B (BMPR1B) and type-2 (BMPR2) and BMPR2 to a lesser extent; fig. S8). Confirming that the growth factors trigger the release of IL-1β by macrophages, in vitro stimulation of macrophages with BMP-2 or PDGF-BB induced the release of IL-1β (Fig. 4C). Together, we show that exposure to IL-1R1 signaling inhibits the response of bone-forming cells (MSCs and osteoblasts) to BMP-2 and PDGF-BB, while local delivery of the growth factors further promotes IL-1R1 signaling via triggering the release of IL-1β by macrophages (Fig. 5).

Engineering of PDGF-BB and IL-1Ra with $PlGF_{123–141}$ to confer super-affinity to ECM proteins

Since we found that IL-1R1 signaling rigorously inhibits the prore-generative effects of BMP-2 and PDGF-BB, we thought to codeliver the growth factors with IL-1 receptor antagonist (IL-1Ra) to promote superior regeneration. First, to optimize delivery, we decided to enhance the affinity of the recombinant proteins to fibrin and endogenous extracellular matrix (ECM) (*2*). BMP-2 is known to have a high binding affinity for fibrin and various ECM proteins (*21*). However, the binding affinity of PDGF-BB for fibrin and other ECM proteins is known to be medium (*21*), and the ability of IL-1Ra to bind ECM proteins is poorly documented. Thus, we engineered PDGF-BB and IL-1Ra to contain a very high affinity ECM/fibrin-binding sequence derived from placenta growth factor (PlGF) (*21*). $PlGF_{123–141}$ was added at the C terminus of PDGF-BB and IL-1Ra to generate PDGF-BB/$PlGF_{123–141}$ and IL-1Ra/$PlGF_{123–141}$ (Fig. 6A). Fusing $PlGF_{123–141}$ to PDGF-BB and IL-1Ra provided very strong binding (i.e., super-affinity) to all ECM proteins tested (fibronectin, vitronectin, tenascin C, and fibrinogen), with 4- to 100-fold increase in affinity (Fig. 6B). Moreover, BMP-2, as well as $PlGF_{123–141}$–fused PDGF-BB and IL-1Ra, was strongly retained in fibrin, while wild-type PDGF-BB and IL-1Ra were quickly released (Fig. 6C). Although BMP-2, PDGF-BB/$PlGF_{123–141}$, and IL-1Ra/$PlGF_{123–141}$ were retained in fibrin, they were gradually released in the presence of the protease plasmin, which cleaves fibrin fibers and $PlGF_{123–141}$ (Fig. 6C) (*2*). Notably, fusing $PlGF_{123–141}$ to PDGF-BB did not alter the activity of the growth factor, since MSC proliferation in response to wild-type PDGF-BB and PDGF-BB/$PlGF_{123–141}$ was similar (fig. S9). Likewise, IL-1Ra was not compromised by the fusion with $PlGF_{123–141}$, since wild-type IL-1Ra and IL-1Ra/$PlGF_{123–141}$ displayed the same inhibitory activity (fig. S9).

Enhanced growth factor–driven bone regeneration with super-affinity IL-1Ra

To test whether local delivery of super-affinity IL-1Ra supports bone regeneration driven by BMP-2 and PDGF-BB, we first used the critical-size calvarial defect model in the mouse. Delivering wild-type IL-1Ra without growth factors slightly enhanced regeneration compared to fibrin-only control, and IL-1Ra/$PlGF_{123–141}$ induced significantly more bone formation compared to wild-type IL-1Ra (Fig. 6, D and E). Codelivering BMP-2 with wild-type IL-1Ra strongly stimulated bone regeneration compared to delivering BMP-2 alone (Figs. 1 and 6, D and E). However, the codelivery of BMP-2 with IL-1Ra/$PlGF_{123–141}$ promoted significantly more bone formation compared to codelivering BMP-2 with wild-type IL-1Ra, leading to nearly 100% coverage of the defect and larger bone volume formation (Fig. 6, D and E). Similarly, the codelivery of

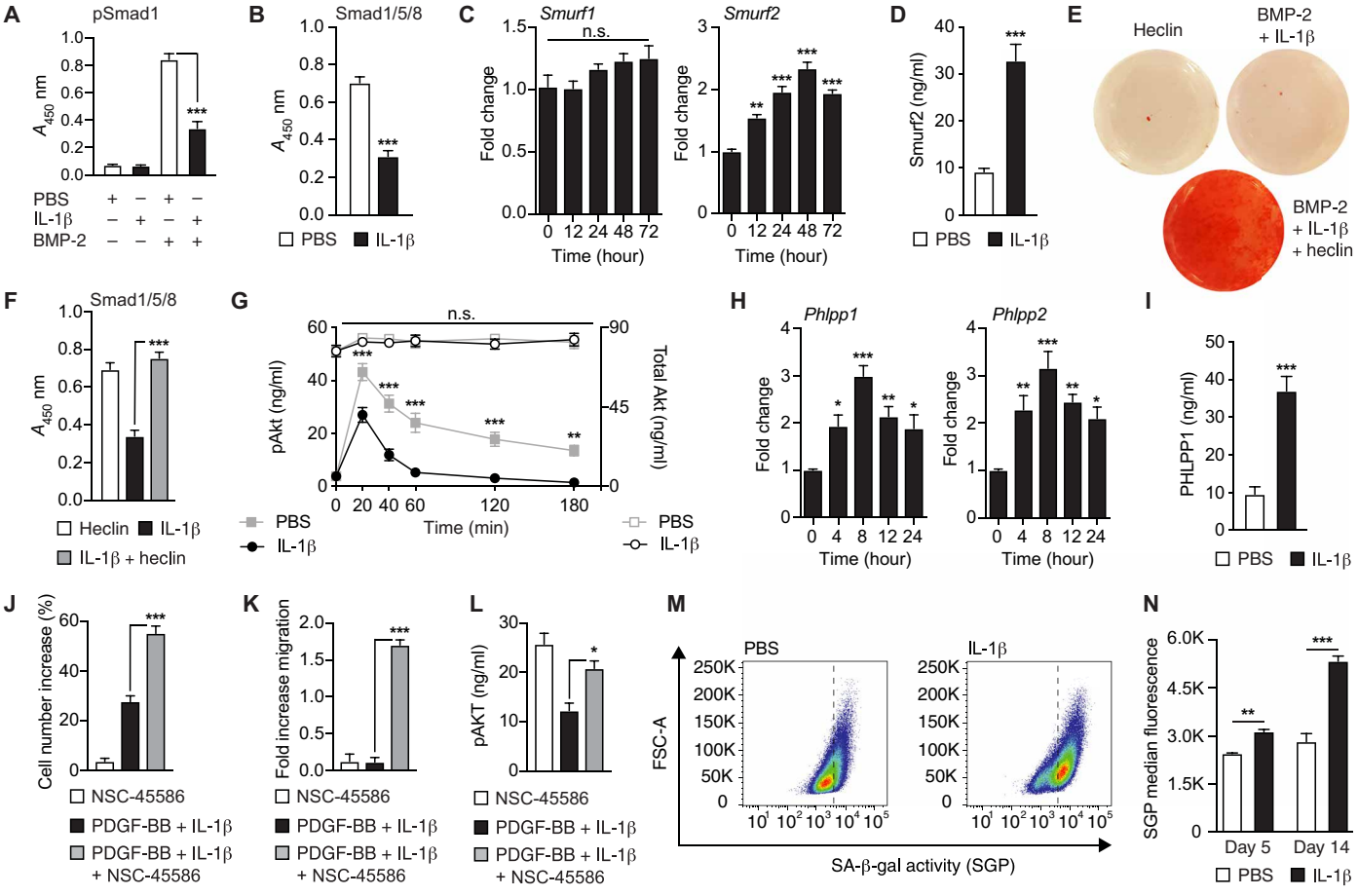

Fig. 3. IL-1β makes cells less responsive to BMP-2 and PDGF-BB signaling. (**A**) Phospho-Smad levels in MSCs pretreated with IL-1β or phosphate-buffered saline (PBS) 30 min after BMP-2 stimulation. $n = 4$. (**B** to **D**) MSCs were treated with IL-1β or PBS. Smad1/5/8 levels after 24 hours in (B). $n = 6$. *Smurf1* and *Smurf2* relative expression in (C). $n = 3$. Smurf2 levels after 24 hours in (D). $n = 4$. (**E**) MSC matrix mineralization in response to BMP-2, IL-1β, and heclin (21 days, representative wells of 2 cm^2). (**F**) Smad1/5/8 levels in MSCs 24 hours after stimulation with IL-1β and heclin. $n = 6$. (**G**) Phospho-Akt (S_{473}, solid squares/circles, left *y* axis) and total Akt (open squares/circles, right *y* axis) in IL-1β–conditioned MSCs stimulated with PDGF-BB. $n = 4$. (**H** and **I**) MSCs were incubated with IL-1β. *Phlpp1* and *Phlpp2* relative expression in (H). $n = 6$. PHLPP1 levels after 24 hours in (I). $n = 4$. (**J**) MSC proliferation in response to PDGF-BB, IL-1β, and NSC-45586 after 72 hours. $n = 6$. (**K**) MSC Transwell migration induced by PDGF-BB, IL-1β, and NSC-45586 (increase over basal migration after 6 hours). $n = 6$. (**L**) Phospho-Akt (S_{473}) levels 120 min after PDGF-BB stimulation of MSCs pretreated with NSC-45586 and IL-1β. $n = 4$. (**M** and **N**) SA-β-gal activity assessed with senescence green probe (SGP) against forward scatter area (FSC-A) in MSCs cultured with IL-1β. Representative flow cytometry plots in (M) and median fluorescence intensities in (N). $n = 3$. For all panels, data are means ± SEM. For (A), (C), (F), (H), and (J) to (L), one-way ANOVA with Bonferroni post hoc test. For (B), (D), (I), and (N), Student's *t* test. For (G), two-way ANOVA with Bonferroni post hoc test. $^*P < 0.05$; $^{**}P < 0.01$; $^{***}P < 0.001$. n.s., not significant.

PDGF-BB/$PlGF_{123–141}$ with IL-1Ra/$PlGF_{123–141}$ significantly improved regeneration compared to the delivery of PDGF-BB/$PlGF_{123–141}$ alone and the codelivery of PDGF-BB/$PlGF_{123–141}$ with wild-type IL-1Ra (Fig. 6, D and E).

Because IL-1Ra inhibits the proinflammatory effect of IL-1β, we then tested whether macrophage polarization during bone regeneration was influenced by the delivery of the antagonist. We focused on the up-regulation of the mannose receptor CD206, since this surface marker is well accepted for detecting M2-like macrophages in tissues (*5*, *22*). In defects treated with fibrin only, the population of CD206-positive macrophages gradually increased during the first 9 days after injury, while defects treated with BMP-2 or PDGF-BB/$PlGF_{123–141}$ displayed a slower increase (fig. S10). Mice treated with IL-1Ra/$PlGF_{123–141}$ displayed a higher percentage of CD206-positive macrophages from days 6 until 14, compared to treatments with fibrin only and wild-type IL-1Ra (fig. S10), suggesting that IL-1Ra/$PlGF_{123–141}$ supports a faster polarization of macrophages toward an anti-inflammatory phenotype.

Last, we tested whether super-affinity IL-1Ra could improve bone regeneration driven by growth factors in a critical-size defect model in the mouse femur. Defects of 2 mm were generated and stabilized with a metallic plate (*23*). Then, BMP-2 and PDGF-BB/$PlGF_{123–141}$ were delivered with or without IL-1Ra/$PlGF_{123–141}$ via fibrin. Codelivering both growth factors with IL-1Ra/$PlGF_{123–141}$ significantly induced the formation of more bone volume after 3 months, compared to delivering the growth factors without IL-1Ra/$PlGF_{123–141}$ (Fig. 6, F and G).

DISCUSSION

Growth factors are powerful tools for regenerative medicine, but their application has been limited by many issues that could probably be

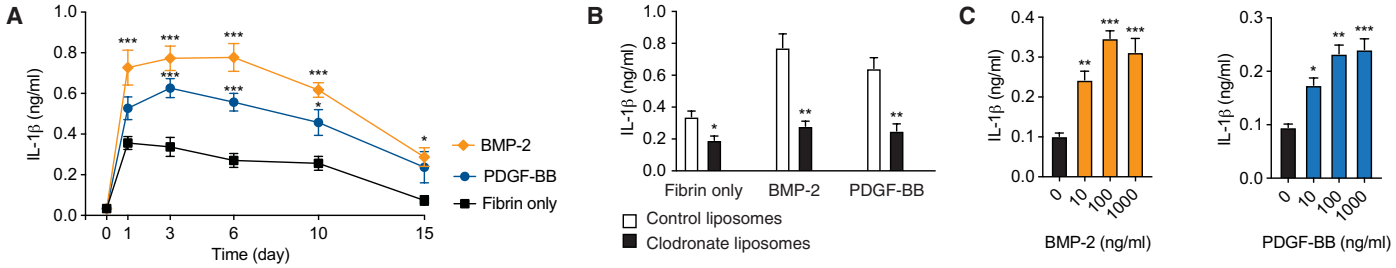

Fig. 4. Delivering BMP-2 and PDGF-BB triggers IL-1β release by macrophages. (**A** and **B**) Calvarial defects were treated with fibrin matrices containing saline (fibrin only), BMP-2, or PDGF-BB (1 μg). Fibrin matrices with bone tissue surrounding the defects were collected at different time points. Graph in (A) shows IL-1β concentration in the harvested samples (IL-1β concentration per milliliter of tissue lysate). $n = 3$ per time point. Graph in (B) shows IL-1β concentrations measured at day 6 in mice with macrophages (control liposomes) or depleted of macrophages (clodronate liposomes). $n = 4$. (**C**) Primary macrophages were treated with BMP-2 or PDGF-BB. IL-1β concentration in the media after 24 hours was measured. $n = 4$. Statistics are between no treatment (0 ng/ml) and treatments. For all panels, data are means ± SEM. For (A), two-way ANOVA with Bonferroni post hoc test. For (B), Student's *t* test. For (C), one-way ANOVA with Bonferroni post hoc test. $^*P < 0.05$; $^{**}P < 0.01$; $^{***}P < 0.001$.

overcome by a better understanding of their signaling dynamics and by optimizing delivery systems. In addition, the response of immune cells to recombinant growth factor delivery is largely elusive but likely very important for optimizing growth factor effectiveness and safety. Actually, the immune system is probably a critical parameter to consider when designing regenerative strategies based on growth factors. Here, we have hypothesized that the regenerative response to growth factors is influenced by the immune and inflammatory microenvironment, which practically always accompanies tissue repair and regeneration (*5*). Because the proinflammatory cytokine IL-1 is a central mediator of inflammation and immunity, we explored the extent to which IL-1R1 signaling affects regeneration driven by growth factors, and we focused on bone as a regeneration system.

Among models commonly used for evaluating bone regeneration, we first chose the critical-size calvarial defect model in the mouse for its reliability and low variability in both basic and applied research (*24*). In addition, this model is ideal to investigate the impact of IL-1R1 signaling during growth factor–driven regeneration, because of the availability of the IL-1R1–deficient mouse. We found that the regenerative effect of recombinant BMP-2 and PDGF-BB is greatly enhanced in *Il1r1*$^{-/-}$ mice, strongly indicating that IL-1R1 signaling impairs the capacity of the growth factors to promote regeneration. Thus, it suggests that blocking IL-1R1 could be used to improve regeneration driven by BMP-2 and PDGF-BB.

In the context of bone regeneration, BMP-2 and PDGF-BB are well known to act on bone-resident MSCs and osteoblasts to promote new bone formation. BMP-2 promotes differentiation, while PDGF-BB promotes chemotaxis and proliferation (*10*). We previously found that MSC proliferation and osteoblastic differentiation is inhibited by IL-1β (*10*). Here, we show that IL-1R1 signaling inhibits the fundamental morphogenic effects triggered by BMP-2 and PDGF-BB. Mechanistically, we propose that exposure to IL-1R1 signaling makes MSCs and osteoblasts less responsive to BMP-2 and PDGF-BB, by two mechanisms. In the context of BMP-2, IL-1R1 signaling increases Smurf2 expression and promotes Smad1/5/8 degradation, which results in an impairment of BMP-2–driven differentiation, due to lower Smad and therefore phospho-Smad levels. In line with this finding, it has been shown that nuclear factor κB (NF-κB), the main transcription factor activated by IL-1R1 signaling, inhibits osteogenic differentiation of MSCs by promoting β-catenin degradation via Smurf2 (*25*, *26*). In the context of PDGF-BB, IL-1R1 signaling increases expression of PHLPPs, which drives quicker Akt dephosphorylation and impairs proliferation and migration responses that are normally induced by PDGF-BB. Similarly, it has been shown that inflammatory mediators signaling via NF-κB also enhance PHLPP1 in human chondrocytes (*27*). Notably, because Smad1/5/8 and Akt are critical in the signaling of many growth factors, activation of IL-1R1 may inhibit not only the activity of recombinant BMP-2 and PDGF-BB but also several other potential therapeutics such as BMPs and growth factors in the vascular, fibroblast, and epidermal growth factors families.

The senescence of cells critical for repair and regeneration, such as stem cells and progenitor cells, is a major hurdle for the healing of musculoskeletal tissues (*28*). Recently, NF-κB has been linked to skeletal stem/progenitor cell senescence and dysfunction in human and mouse (*29*). Here, in addition to the negative effects of IL-1R1 signaling in growth factor signaling, we show that long-term activation (1 to 2 weeks) of IL-1R1 accelerates MSC senescence, as SA-β-gal activity in MSCs was enhanced over time when cells were treated with IL-1β. While the exact signaling mechanisms involved in IL-1R1–driven senescence are still unclear, the enhanced expression of Smurf2 following IL-1R1 activation is probably important, since it has been shown that Smurf2 activity is strongly linked with cellular senescence (*16*–*18*).

We found that the delivery of BMP-2 and PDGF-BB in bone defects significantly increases IL-1β concentration in the injured tissue. The increase of IL-1β is likely due to macrophage response to BMP-2 and PDGF-BB, since IL-1β concentration was not enhanced by delivering the growth factors in mice depleted of monocytes and macrophages. Thus, the detrimental effect of IL-1R1 signaling in MSCs and osteoblasts is probably exacerbated in vivo by macrophages responding to the delivery of recombinant BMP-2 and PDGF-BB. Actually, the effects of BMP-2 and PDGF-BB on monocytes and macrophages are still unclear. For instance, it has been shown that BMP-2 and PDGF-BB induce monocyte and macrophage chemotaxis (*7*, *8*, *30*, *31*). In addition, BMP-2 may modulate the polarization of macrophages toward an anti-inflammatory phenotype either positively or negatively (*8*, *32*). Nevertheless, one of the major side effects of BMP-2 in clinical use is rampant inflammation (*33*–*35*). Here, our data suggest that macrophage response to BMP-2 and PDGF-BB triggers the release of IL-1β, which encourages inflammation.

Because IL-1β inhibits the proregenerative effects of BMP-2 and PDGF-BB and since both growth factors further trigger IL-1β release by macrophages, we thought of codelivering them with IL-1Ra

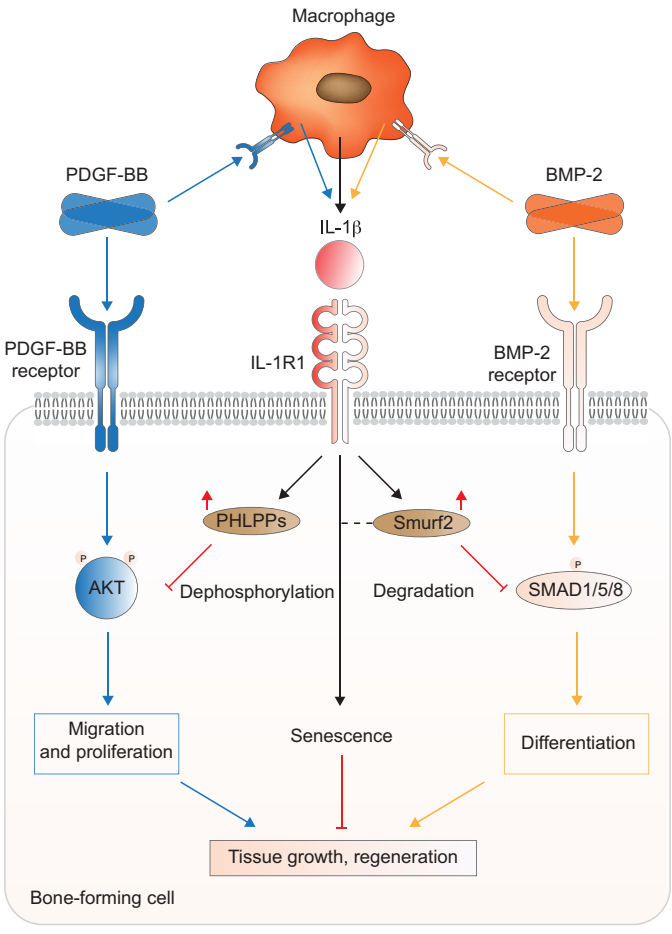

Fig. 5. Proposed mechanism by which IL-1R1 signaling desensitizes bone-forming cells to growth factors. IL-1R1 signaling in bone-forming cells (MSCs and osteoblasts) stimulates the expression of PHLPPs and Smurf2. Higher levels of PHLPPs promote quicker dephosphorylation of Akt and dampen PDGF-BB signaling. Higher levels of Smurf2 impair the responsiveness of cells to BMP-2 by promoting ubiquitination and thus degradation of Smad1/5/8. IL-1R1 signaling also accelerates senescence likely via Smurf2. BMP-2 and PDGF-BB further stimulate IL-1β release by macrophages. Phosphorylation is indicated by small circles with the letter P.

to enhance bone regeneration. Recombinant BMP-2 and PDGF-BB are both USFDA-approved to promote bone formation (*34*, *36*). However, BMP-2 and PDGF-BB have raised major concerns regarding safety and cost-effectiveness for multiple clinical applications, likely due to the use of high doses coupled with suboptimal delivery systems (*2*, *3*, *34*). IL-1Ra (anakinra, Kineret) is approved for the treatment of rheumatoid arthritis and neonatal-onset multisystem inflammatory disease (*37*). Yet, IL-1Ra needs to be used at very high doses (>100 mg per injection) with multiple bulk administrations, and the use of this immunosuppressant has been reported to lead to infections and immunogenicity (*37*). Thus, considering the overall clinical efficacy of recombinant BMP-2, PDGF-BB, and IL-1Ra, better delivery systems need to be developed to allow precise localization and retention of low doses of the drugs at the delivery sites. One of the strategies is to engineer recombinant proteins to strongly bind a biomaterial carrier and endogenous ECM present in the tissue where they are delivered. We have previously demonstrated that this can be achieved by fusing growth factors to $PlGF_{123–141}$, which confers super-affinity to ECM components and ECM-derived biomaterials such as fibrin (*21*). Because PDGF-BB and IL-1Ra naturally have a relatively low affinity for ECM components and fibrin, we engineered them to include $PlGF_{123–141}$, while we decided to use BMP-2 in its wild-type form as it naturally binds many ubiquitous ECM proteins with high affinity (*21*). This strategy allows super-affinity PDGF-BB and IL-1Ra as well as BMP-2 to be retained in a fibrin matrix and released "on demand" via proteases, which naturally cleave both fibrin fibers and the $PlGF_{123–141}$ sequence (*21*).

To test all treatment combinations, we first used the mouse calvarial defect model, because of its simplicity and reliability for evaluating bone regenerative strategies (*24*). Then, to test the most effective treatments, we moved to a mouse femur critical-size defect model for its higher clinical relevance (*23*). Delivering low doses of wild-type BMP-2 (≤1 μg per defect) without a particular delivery system or osteoinductive biomaterial is known to have a modest regenerative effect in calvarial defects (*21*, *38*). A low dose of wild-type PDGF-BB (≤1 μg per defect), which is known to be less potent than BMP-2 for bone regeneration, usually has no significant effect (*39*, *40*). As expected, we observed that wild-type BMP-2 triggers regeneration to some extent, but we found that the super-affinity versions of PDGF-BB and IL-1Ra have greater regenerative capacity compared to their wild-type forms. The enhanced activity of engineered PDGF-BB and IL-1Ra is likely due to their much higher binding affinity to fibrin and endogenous ECM proteins and therefore higher retention at the delivery site (*21*). We demonstrated that codelivering BMP-2 with super-affinity IL-1Ra or codelivering super-affinity PDGF-BB with super-affinity IL-1Ra significantly stimulates superior bone regeneration compared to the delivery of BMP-2 or super-affinity PDGF-BB alone. Furthermore, we confirmed that the regenerative capacity of the growth factors (i.e., formation of new bone tissue) is enhanced by super-affinity IL-1Ra in the femur defect model. Thus, the results in both models clearly show that inhibiting IL-1R1 signaling via a super-affinity IL-1Ra enhances the bone regenerative response to BMP-2 and PDGF-BB. Several strategies based on the delivery of recombinant BMP-2 via hydrogels have been shown to regenerate bone defects in various animal models. For example, a midrange dose of BMP-2 (5 μg) delivered with an electrospun nanofiber mesh and alginate hydrogel was able to promote critical-size femur defect regeneration in the rat (*41*). Lower doses of BMP-2 have also been shown to be effective to heal bone defects, when combined with integrin-binding peptides or domains derived from ECM proteins. For instance, BMP-2 has been delivered via a protease-degradable poly(ethylene glycol) hydrogel functionalized with a triple helical $\alpha_2\beta_1$ integrin–specific peptide (*42*) or a via fibrin matrix functionalized with an $\alpha_5\beta_1$ integrin–specific fibronectin fragment (*38*) to regenerate mouse radius bone and rat calvarial defects, respectively. These strategies, among others, could probably benefit from the inhibition of IL-1R1 signaling for further optimization and for lowering the doses of growth factors.

Macrophage polarization from an inflammatory to an anti-inflammatory state is well known to be important for tissue healing (*5*). Therefore, we also tested whether the delivery of IL-1Ra affects macrophage polarization. Mice treated with super-affinity IL-1Ra displayed a higher percentage of anti-inflammatory-like macrophages, which are commonly characterized by the surface expression of CD206 (*5*, *22*). This suggests that, in addition to restoring BMP-2 and PDGF-BB signaling in MSCs and osteoblasts, super-affinity IL-1Ra may also

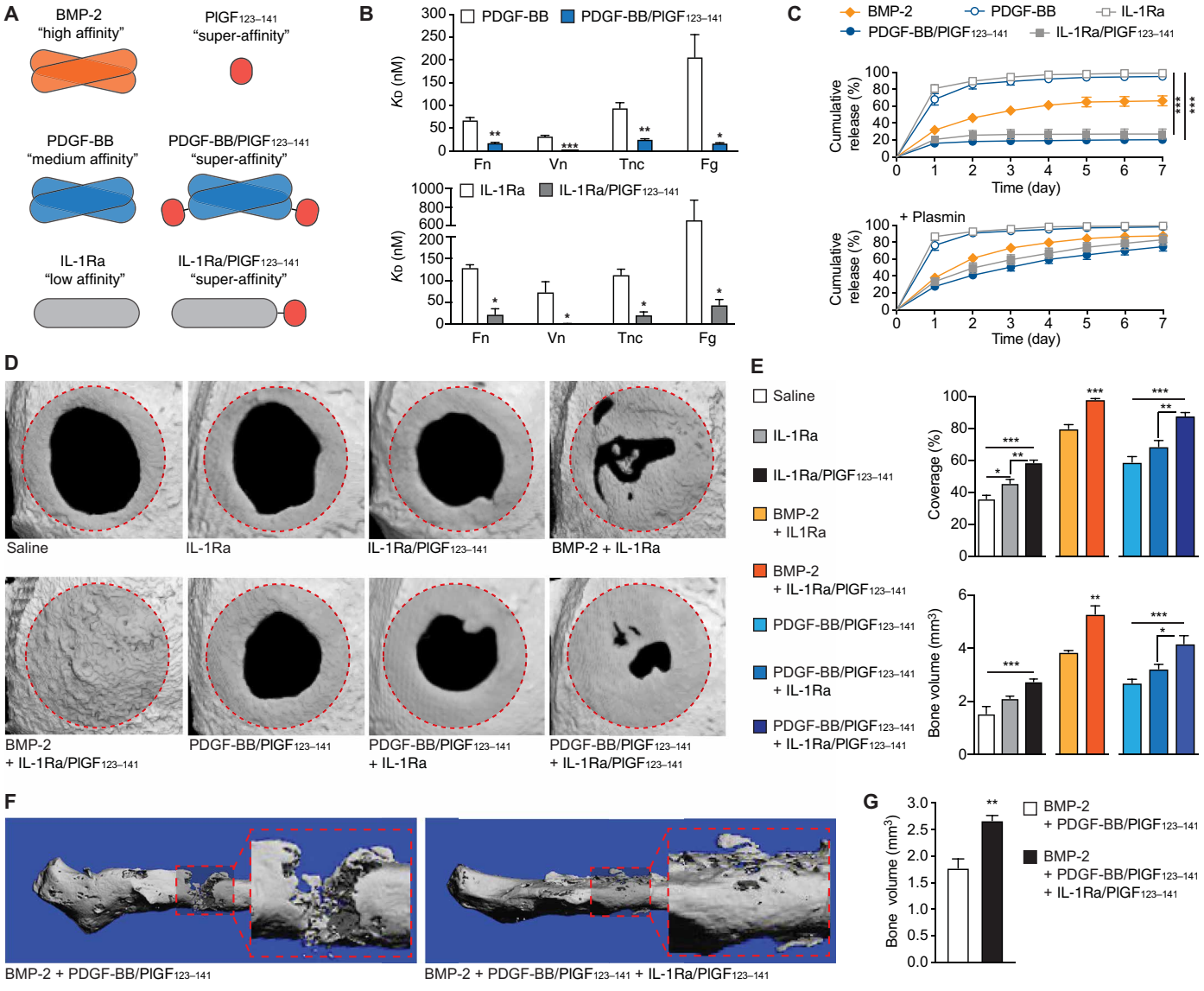

Fig. 6. Super-affinity IL-1Ra enhances the regenerative capacity of BMP-2 and PDGF-BB. (**A**) Design of super-affinity PDGF-BB and IL-1Ra. Affinity for ECM is high for BMP-2, medium for PDGF-BB, and low for IL-1Ra. $PlGF_{123–141}$ is added to the C terminus of PDGF-BB and IL-1Ra to confer super-affinity for ECM. (**B**) Dissociation constant (K_d) of wild-type and $PlGF_{123–141}$-fused proteins for fibronectin (Fn), vitronectin (Vn), tenascin-C (Tnc), and fibrinogen (Fg). $n = 3$. (**C**) Fibrin matrices containing growth factor and IL-1Ra variants were incubated in buffer (containing or not plasmin) that was changed every day. Graphs show cumulative release of the recombinant proteins. $n = 3$. (**D** and **E**) Calvarial defects (4.5-mm diameter) were treated with growth factor (1 μg) and IL-1Ra (1 μg) variants delivered with fibrin. Regeneration was measured by microCT after 8 weeks. Representative calvarial reconstructions (average of the individual samples) in (D). Original defect area is shaded with a dashed outline. Defect coverage and new bone volume in (E). $n = 6$. (**F** and **G**) Femoral defects (2 mm wide, dashed boxes) were treated with growth factors (1 μg) and IL-1Ra/$PlGF_{123–141}$ (1 μg) in fibrin. Regeneration was measured by microCT after 12 weeks. Representative femur reconstructions in (F). New bone volume formed in (G). $n = 5$. For all panels, data are means ± SEM. For (B), (E) (BMP-2 groups), and (G), Student's *t* test. For (C), two-way ANOVA with Bonferroni post hoc test. For (E), one-way ANOVA with Bonferroni post hoc test. *$P < 0.05$; **$P < 0.01$; ***$P < 0.001$.

promote bone regeneration by supporting macrophages polarization toward an anti-inflammatory phenotype.

The strategy of locally inhibiting IL-1R1 with IL-1Ra/$PlGF_{123–141}$ to support the regenerative activity of BMP-2 or PDGF-BB shows very promising results in murine models. As this approach is relatively simple and does not require the delivery of cells, its application could be facilitated compared to stem cell–based strategies. However, before translation to the clinic, such a system needs to be validated in larger animals such as the sheep, which presents a bone structure more similar to humans, with analyses of the mechanical proprieties of the bone tissue formed. The system may also be evaluated in other models of bone formation such as spinal (for BMP-2) and foot/ankle (for PDGF-BB) fusion (*34*, *43*). Nevertheless, because the wild-type forms of the growth factors and IL-1Ra have been clinically approved, translation of this strategy could be facilitated.

In conclusion, we highlight the importance of considering inflammation and the immune system when using growth factors for regenerative medicine applications. Integrating a control of immune

pathways in regenerative therapies based on growth factors could be as important as having smart delivery systems that control growth factor localization and release. In the context of bone regeneration, we demonstrate that an engineered matrix-binding form of IL-1Ra considerably improves the regenerative efficiency of recombinant BMP-2 and PDGF-BB. This strategy may be used not only for bone regeneration and formation but also in chronic bone inflammatory conditions or in other tissues where IL-1R1 signaling has a negative impact.

MATERIALS AND METHODS

Study design

This study was designed to understand the role of IL-1R1 signaling in growth factor–driven regeneration, with the goal of designing new regenerative strategies that integrate control of the immune system. Statistical methods were not used to predetermine required sample size, but sample sizes were determined on the basis of estimates from previously published results such that appropriate statistical tests could yield significant results. All in vitro experiments were replicated at least three times independently. For animal studies, mice were randomized into treatment groups. Treatments of bone defects and analyses were performed in a blinded fashion. The *n* values used to calculate statistics are indicated in the figure legends. Statistical methods are described in the "Statistical analysis" section.

Mice

Wild-type C57BL/6 mice were obtained from the Monash Animal Research Platform or Japan SLC. *Il1r1*$^{-/-}$ mice were backcrossed onto a C57BL/6 background for more than eight generations. Animals were kept under specific pathogen–free conditions. All animal experiments were conducted in accordance with the Monash University guidelines and approved by the local ethics committee or the Animal Research Committee of the Research Institute for Microbial Diseases of Osaka University.

Calvarial defect model

Mice used for surgery were 10 to 12 weeks old. Mice were anesthetized with isoflurane, and the top of their heads was shaved. A longitudinal incision was performed to reveal the skull, and bone tissue was exposed by retracting the soft tissues. Using a drill, two craniotomy defects (4.5-mm diameter) were created in the parietal bones of the skull on each side of the sagittal suture line. The defects were washed with saline and covered with a fibrin matrix polymerized atop the dura [40 μl per defect, fibrinogen (14 mg/ml; Enzyme Research Laboratories), bovine thrombin (4 U/ml; Sigma-Aldrich), 5 mM $CaCl_2$, and aprotinin (25 μg/ml; Roche)]. In selected conditions, 1 μg of growth factor and IL-1Ra variants were added in the matrix. Then, the soft tissue was closed with sutures. As a painkiller, mice received a subcutaneous injection of buprenorphine (0.1 mg/kg). Mice were euthanized 8 weeks after surgery, and the skulls were analyzed by micro–computed tomography (microCT).

Micro–computed tomography

Skulls were scanned with a microCT 40 (Scanco Medical AG) operated at an energy of 55 kilovolt peak (kVp) and an intensity of 145 ms for detailed measurements. Scans were reconstructed with a nominal isotropic resolution of 30 μm. After reconstruction, a three-dimensional (3D) Gaussian filter (sigma, 1.2; support, 1) was applied to all images. Bone was segmented from background using a global threshold of 22.4% of maximum gray value. Afterward, cylindrical masks were placed manually at the defects. Bone coverage and volume within these masks were calculated using the scanner software [Image Processing Language (IPL), Scanco Medical AG]. Coverage was calculated on a dorso-ventral projection of the cylindrical area. Femurs were scanned in ethanol with the same microCT operated at an energy of 55 kVp and an intensity of 145- and 300-ms integration time for detailed measurements. Scans were performed at a high-resolution mode, resulting in a nominal isotropic resolution of 15 μm. After reconstruction, a 3D Gaussian filter (sigma, 1.2; support, 1) was applied to all images. Images were rotated to align the longitudinal axis of the bone to the *y* axis of the image. Bone was segmented from background using a global threshold of 31.6% of maximum gray value and a region of interest of 250 × 320 × 250 voxels selected centrally at the defect region. Bone volume was calculated using the scanner software (IPL, Scanco Medical AG).

Compact bone–derived MSC isolation

All muscle and cartilage tissue from long bones (arms and legs) of C57BL/6 and *Il1r1*$^{-/-}$ mice (6 to 8 weeks old) were removed and briefly submerged in 70%, before being washed in phosphate-buffered saline (PBS). The epiphysis of each bone was cut off, and bone marrow was flushed using a 27-gauge needle attached to a 10-ml syringe filled with PBS. The cleaned bones were cut into 1- to 2-mm chips and digested for 1 hour at 37°C in 5 ml of α–minimum essential medium (α-MEM) containing collagenase II (1 mg/ml; Merck). Chips were washed with α-MEM [with 10% fetal bovine serum (FBS)], evenly distributed on a cell culture dish (one 10-cm^2 dish per mouse), and covered with 6 ml of culture media [α-MEM, penicillin/streptomycin (100 mg/ml), 2 mM GlutaMax, and 10% FBS]. Chips were incubated at 37°C, 5% CO_2 for 10 days, allowing cells to migrate out and adhere on the surface. Media was changed at day 5. Cells and chips were washed with PBS, harvested with 0.25% trypsin/EDTA, and transferred to cell culture dishes (two 21-cm^2 dishes per mouse). Cells were grown to 80% confluence and transferred without the chips in flasks (one 175-cm^2 flask per mouse). MSCs were expanded for two passages with a 1:4 split ratio and stored in liquid nitrogen. MSC phenotype was assessed by staining cells with TruStain FcX anti-CD16/32 (1 μg/ml; clone 93, BioLegend) and LIVE/DEAD Zombie Aqua (1:500 dilution; BioLegend). Then, cells were labeled with the following antibodies from BioLegend: anti-CD11b phycoerythrin (PE) (2 μg/ml; clone M1/70), CD45 fluorescein isothiocyanate (FITC) (5 μg/ml; clone 30-F11), anti–major histocompatibility complex II allophycocyanin (APC)–Cy7 (1 μg/ml; clone M5/114.15.2), anti-CD44 APC-Cy7 (2 μg/ml; clone IM7), anti-CD29 PE (2 μg/ml; clone HMβ1-1), anti-CD90.2 APC (2 μg/ml; clone 30-H12), anti-CD140b APC (2 μg/ml; clone APB5), anti–Sca-1 PE (2 μg/ml; clone D7), and anti–IL-1R1 (2 μg/ml; clone JAMA-147). Anti-CD19 APC from BD Pharmingen (clone 1D3) was used at 2 μg/ml. Antibodies were diluted in flow cytometry buffer [PBS, 5 mM EDTA, and 1% bovine serum albumin (BSA)]. Samples were acquired on CyAn ADP (Beckman Coulter) and analyzed with FlowJo software (TreeStar Inc.).

Osteoblast isolation

Calvariae of C57BL/6 3-days-old mice were digested in α-MEM containing collagenase type II (1 mg/ml; Merck) and dispase (2 mg/ml; Sigma-Aldrich) at 37°C for 20 min in a shaking water bath to release calvarial cells. The supernatant containing released cells was transferred to a new tube and centrifuged at 300*g*, and the pellet was resuspended

in α-MEM containing penicillin/streptomycin (100 mg/ml) and 10% FBS. The calvariae were digested three more times for a total of four digestions. Digestions 3 and 4 containing osteoblasts were combined together and transferred in a tissue culture–treated dish at a density of 3×10^5 cells/ml. Calvarial cells were maintained in culture for 2 weeks in osteogenesis induction medium [α-MEM with 2 mM L-glutamine, 10% FBS, penicillin/streptomycin (100 mg/ml), 50 μM ascorbate phosphate, 10 mM β-glycerophosphate, and BMP-2 (50 ng/ml)] and stored in liquid nitrogen before use.

Matrix mineralization

MSCs (passage 3) were seeded in 24-well plates (10,000 cells per well) with 750 μl of osteoblast differentiation medium [α-MEM with 2 mM L-glutamine, 10% FBS, penicillin/streptomycin (100 mg/ml), 50 μM ascorbate phosphate, and 10 mM β-glycerophosphate] with BMP-2 (50 ng/ml) and/or murine IL-1β (1 ng/ml; PeproTech). For the Smurf2 inhibition experiment, 20 μM heclin (R&D Systems) was added in the medium. After 5 days, osteogenesis-inducing medium was replaced without IL-1β or heclin. The medium was changed every 4 days until day 21. To determine the degree of mineralization, medium was removed and the wells washed once with PBS. Cells were fixed with 10% formalin at room temperature for 1 hour, and wells were washed with water before being stained with 2% alizarin red for 20 min. Alizarin red was aspirated, and wells were washed twice with water before being photographed.

Quantitative polymerase chain reaction for osteoblastic differentiation

Cells (MSCs passage 3 or osteoblasts) were seeded in 24-well plates (10,000 cells per well) with 750 μl of osteogenesis inducing medium [α-MEM with 2 mM L-glutamine, 10% FBS, penicillin/streptomycin (100 mg/ml), 50 μM ascorbate phosphate, and 10 mM β-glycerophosphate] containing BMP-2 (50 ng/ml) with or without murine IL-1β (1 ng/ml). After 5 days, osteogenesis-inducing medium was replaced (without IL-1β). Media was changed every 4 days. Seven or 14 days following stimulation with IL-1β, total RNAs were isolated, using the RNeasy Plus Mini Kit (Qiagen), and reverse transcription was performed using ReverTra Ace (Toyobo Co. Ltd.). Quantitative polymerase chain reaction (PCR) was performed with an ABI Prism 7500 using TaqMan assay. The following primers from Applied Biosystems were used: *Alpl* mouse, Mm00475834_m1; *Runx2* mouse, Mm00501580_m1; *Ibsp* mouse, Mm00492555_m1; Eukaryotic 18S rRNA Endogenous Control (VIC/MGB Probe, Primer Limited).

MSC colony formation

Fresh MSCs were seeded in six-well plates (100 cells per well) and grown in 6 ml of α-MEM [containing penicillin/streptomycin (100 mg/ml), 2 mM GlutaMax, and 10% FBS] with or without IL-1β (1 ng/ml) and PDGF-BB (10 ng/ml) for 5 days. Media was changed once, and cells were cultured for five more days. To assess colony formation, media was aspirated, and plates were rinsed with PBS. Then, cells were stained in 3% crystal violet solution in methanol for 10 min. The plates were washed with water until excess crystal violet was removed. The number of colonies (more than 50 cells, determined by light microscopy) was counted, and their size was measured using ImageJ software.

Cell proliferation assays

Cells (MSCs passage 3 or osteoblasts) were starved for 24 hours in low-serum α-MEM [penicillin/streptomycin (100 mg/ml), 2 mM GlutaMax, and 1% FBS]. Then, cells were seeded in a 96-well plate (1500 cells per well) with low-serum α-MEM containing PDGF-BB (10 ng/ml) and/or murine IL-1β (1 ng/ml; PeproTech). For the PHLPP inhibition experiment, medium contained 20 μM NSC-45586 (Aobious). For the experiment with IL-1Ra variants, IL-1Ra (R&D Systems) or IL-1Ra/PlGF$_{123–141}$ (10, 100, or 1000 ng/ml) was added to the medium. For the experiment with PDGF-BB variants, medium contained only PDGF-BB or PDGF-BB/PlGF$_{123–141}$ (1, 5, or 20 ng/ml). Percentage of new cells was calculated over basal proliferation (low-serum α-MEM only) using CyQuant (Thermo Fisher Scientific) and the equation [(cell number in basal proliferation group/cell number in stimulation group) − 1] × 100.

Migration assays

Low-serum α-MEM [penicillin/streptomycin (100 mg/ml), 2 mM GlutaMax, and 1% FBS] containing murine PDGF-BB (10 ng/ml) with or without murine IL-1β (1 ng/ml) was added to the bottom side of a collagen type I (C4243, Sigma-Aldrich)–coated Transwell (8-μm pore size, Millipore). For PHLPP inhibition experiments, medium contained 20 μM NSC-45586 (Aobious). Directly after, cells (30,000 cells in 200 μl) were added onto the Transwell upper chambers. After 6 hours, membranes of each insert were removed and mounted on microscopy glass slides using Vectashield mounting medium containing 4′,6-diamidino-2-phenylindole (Vector Laboratories). The number of cells that migrated to the bottom side of the membrane was counted in three random fields using a fluorescent microscope. Fold increase in migration was calculated over basal migration (bottom chamber with medium only).

Phospho-Smad assay

Cells (MSCs passage 3 or osteoblasts) were seeded in six-well plates and cultured until 70% confluency with α-MEM [penicillin/streptomycin (100 mg/ml), 2 mM GlutaMax, and 10% FBS]. Then, cells were starved for 24 hours with low-serum α-MEM (2% FBS), before being stimulated with PBS or murine IL-1β (1 ng/ml; PeproTech). Cells were kept in culture for further 24 hours and stimulated with BMP-2 (20 ng/ml) or PBS control for 30 min. Relative pSmad1 levels were assessed with the SMAD1 (Phospho) (pS463/pS465) InstantOne ELISA Kit (Thermo Fisher Scientific) according to the manufacturer's instructions.

Smad protein assay

Cells (MSCs passage 3 or osteoblasts) were seeded in six-well plates and cultured until 70% confluency with α-MEM [penicillin/streptomycin (100 mg/ml), 2 mM GlutaMax, and 10% FBS]. Cells were then starved with low-serum α-MEM (2% FBS). After 24 hours, cells were stimulated with PBS or murine IL-1β (1 ng/ml; PeproTech). For the Smurf2 inhibition experiment, 20 μM heclin (R&D Systems) was added to the medium. After additional 24 hours, Smad1/5/8 relative levels were assessed using a sensitive enzyme-linked immunosorbent assay (ELISA) kit according to the manufacturer's instructions (Signosis, TE-0015).

SMURF and PHLPP quantitative PCRs

Cells (MSCs passage 3 or osteoblasts) were seeded in six-well plates and cultured until 70% confluency with α-MEM [penicillin/streptomycin (100 mg/ml), 2 mM GlutaMax, and 10% FBS]. Then, cells were starved for 24 hours with low-serum α-MEM (2% FBS), before being stimulated with murine IL-1β (1 ng/ml; PeproTech) for 0 to

72 hours (Smurf experiment) or for 0 to 24 hours (PHLPP experiment). Total RNA was isolated using the RNeasy Plus Mini Kit (Qiagen), and reverse transcription was performed using ReverTra Ace (Toyobo Co. Ltd.). Quantitative PCR was performed with an ABI Prism 7500 using TaqMan assay with the following primers: *Smurf1*, Mm00547102_m1; *Smurf2*, Mm03024086_m1; *Phlpp1*, Mm01295850_m1; *Phlpp2* mouse, Mm01244267_m1; Eukaryotic 18S rRNA Endogenous Control (VIC/MGB Probe, Primer Limited) (Applied Biosystems).

SMURF2 and PHLPP1 quantification

Cells (MSCs passage 3 or osteoblasts) were seeded in six-well plates and cultured until 70% confluency with α-MEM [penicillin/streptomycin (100 mg/ml), 2 mM GlutaMax, and 10% FBS]. Cells were then starved with low-serum α-MEM (2% FBS). After 24 hours, cells were stimulated with PBS or murine IL-1β (1 ng/ml; PeproTech). After additional 24 hours, Smurf2 and PHLPP1 were quantified using ELISA (Mouse E3 Ubiquitin-Protein Ligase SMURF2 and Mouse PH Domain Leucine-Rich Repeat-Containing Protein Phosphatase 1 ELISA Kits, MyBioSource) according to the manufacturer's instructions.

Akt phosphorylation assay

Cells (MSCs passage 3 or osteoblasts) were seeded in six-well plates and cultured until 70% confluency with α-MEM [penicillin/streptomycin (100 mg/ml), 2 mM GlutaMax, and 10% FBS]. Cells were starved for 24 hours with low-serum α-MEM before being stimulated with PBS or murine IL-1β (1 ng/ml; PeproTech) for 4 hours. Then, murine PDGF-BB (10 ng/ml) was added in the medium for 0 to 180 min. For PHLPP inhibition experiments, 20 μM NSC-45586 (Aobious) was added in the medium. Total Akt and phosphorylated Akt were quantified by ELISA [Phospho-Akt (S_{473}) Pan Specific DuoSet IC, R&D Systems] according to the manufacturer's instructions.

SA-β-gal assay

MSCs (passage 4) were seeded at 3000 cells/cm^2 in α-MEM [penicillin/streptomycin (100 mg/ml), 2 mM GlutaMax, and 5% FBS] containing IL-1β (1 ng/ml; PeproTech). Media was changed every 3 days, and cells were used for senescence analysis on days 5 and 15. Cells seeded for day 15 were passaged twice during the treatment duration to avoid overconfluency. At the indicated time points, cells were harvested using TrypLE Express (Gibco) and first stained with the LIVE/DEAD Fixable Aqua Dead Cell Stain Kit (1:500 diluted in PBS; Invitrogen) for 30 min at 4°C. Then, SA-β-gal activity was measured, using the CellEvent Senescence Green Flow Cytometry Assay Kit (Invitrogen, #C10840), according to the manufacturer's instructions. Briefly, cells were fixed with paraformaldehyde (2% in PBS) for 15 min at room temperature. Then, cells were washed with PBS containing 1% BSA and further stained with the CellEvent Senescence Green Probe (diluted 1:500 in prewarmed CellEvent Senescence Buffer) for 2 hours at 37°C without CO_2. After incubation, cells were washed with PBS containing 1% BSA and resuspended in flow cytometry buffer (PBS with 1% BSA and 5 mM EDTA) for analysis on BD LSRFortessa X-20. The postacquisition analysis was done using FlowJo software (TreeStar Inc.).

Senescence-associated cytokine detection

MSCs (passage 4) were seeded at in six-well plates at 70% confluency in α-MEM [penicillin/streptomycin (100 mg/ml), 2 mM GlutaMax, and 2% FBS] and stimulated with IL-1β (5 ng/ml). After 48 hours, cytokines in the media were detected using an antibody array (Mouse Cytokine Array Panel A, R&D Systems) according to the manufacturer's instructions. The assay was done with 400 μl of cell culture supernatant. The chemiluminescent signals were detected using ImageQuant LAS 4000 and quantified with ImageQuant TL software (GE Healthcare Life Sciences).

Surface expression of growth factor receptors on MSCs

MSCs (passage 4) were seeded in six-well plates at 70% confluency in α-MEM [penicillin/streptomycin (100 mg/ml), 2 mM GlutaMax, and 2% FBS] and stimulated with IL-1β (1 ng/ml). After 1 day, cells were detached and stained with the LIVE/DEAD Fixable Aqua Dead Cell Stain Kit (1:500 diluted in PBS; Invitrogen) for 30 min at room temperature. Then, cells were incubated in the blocking buffer (10 μg/ml; TruStain FcX anti-CD16/32, clone 93, BioLegend, and 5% heat-inactivated FBS) for 30 min on ice. Cells were stained with FITC anti-CD140a (3 μg/ml; PDGFRα, clone APA5, Miltenyi Biotec), APC anti-CD140b (2 μg/ml; PDGFRβ, clone APB5, BioLegend), Alexa Fluor 488 anti-BMPR1A (5 μg/ml; C32447, Signalway Antibody), Alexa Fluor 647 anti-BMPR1B (2 μg/ml; C32547, Signalway Antibody), Alexa Fluor 488 anti-BMPR2 (5 μg/ml; C32961, Signalway Antibody), or Alexa Fluor 647 anti-ACVR1 (2 μg/ml; C43627, Signalway Antibody). Cells were acquired on an LSRFortessa X-20 and analyzed with FlowJo software (TreeStar Inc.).

Release of IL-1β following bone injury

Calvarial defects (4.5-mm diameter) in C57BL/6 mice were treated with a fibrin matrix as described for the calvarial defect model with 1 μg of murine BMP-2 or PDGF-BB (PeproTech). After 1, 3, 6, 10, and 15 days, the partially remodeled matrix and the bone tissue surrounding the defect (1 mm farther) was collected. As a control, a 4.5-mm-diameter calvarial bone tissue was collected (day 0). Fibrinous matrices and tissue samples were incubated in 1 ml of tissue protein extraction reagent (T-PER, Thermo Fisher Scientific) containing protease inhibitors [1 tablet of protease inhibitor cocktail (Roche) for 10 ml] and homogenized with a tissue homogenizer. Tissue lysates were incubated for 1 hour at 4°C and centrifuged at 5000*g* for 5 min, before being stored at −80°C. Cytokines were detected by ELISA (Mouse IL-1β/IL-1F2 DuoSet, R&D Systems) according to the manufacturer's instructions.

Macrophage depletion

One day before surgery, 200 μl of clodronate liposomes (5 mg/ml) or empty liposomes (Liposoma) was intravenously injected in C57BL/6 mice (10 to 12 weeks old). An additional 200 μl of clodronate liposomes or empty liposomes were intraperitoneally injected every 2 days until day 6. Mouse spleens were harvested and crushed, and red blood cells were lysed with red blood cell lysis buffer [ammonium chloride (8.3 g/liter) and 10 mM tris-HCl in distilled water]. Macrophage depletion was verified by resuspending splenocytes in TruStain FcX anti-CD16/32 (1 μg/ml; clone 93, BioLegend) antibodies to block nonspecific binding and 1:500 dilution of Zombie Aqua (BioLegend) diluted in PBS. Subsequently, splenocytes were labeled with the following antibodies: anti-CD11b PE (1 μg/ml; clone M1/70, BioLegend), anti-Ly6G BV421 (1 μg/ml; clone 1A8, BioLegend), and anti-F4/80 biotin (3 μg/ml; clone REA126, Miltenyi Biotech) conjugated to streptavidin APC/Fire 750 (0.4 μg/ml; BioLegend) diluted in flow cytometry buffer (PBS with 1% BSA and 5 mM EDTA). Samples were acquired

on a BD FACS Fortessa X20 and analyzed with FlowJo software (TreeStar Inc.).

Macrophage stimulation with growth factors and detection of growth factor receptors

Bone marrow from femora and tibiae of C57BL/6 mice (8 to 12 weeks) was flushed out with Dulbecco's modified Eagle's medium/Nutrient Mixture (DMEM/F12 medium, Gibco) using a 27-gauge needle and a 10-ml syringe. Cells were filtered through a 70-μm nylon strainer, centrifuged at 500*g* for 10 min at 4°C, and resuspended in DMEM/F12 medium containing 10% heat-inactivated FBS, penicillin/streptomycin (100 mg/ml), and 20% L929 fibroblast–conditioned medium. Cells were plated in 150-mm-diameter petri dishes at a density of 5×10^7 and cultured for 7 days at 37°C and 5% CO_2. Medium was replaced every 3 days. After 7 days, macrophages were detached using TrypLE (Gibco) containing 3 mM EDTA and seeded in 12-well plates at a density of 2×10^5 cells per well in DMEM/F12 with 10% heat-inactivated FBS and penicillin/streptomycin (100 mg/ml). After 1 day, macrophages were detached and stained with TruStain FcX anti-CD16/32 (1 μg/ml; clone 93, BioLegend) and the LIVE/DEAD Fixable Aqua Dead Cell Stain Kit (1:500 diluted in PBS; Invitrogen) for 30 min at room temperature. Then, cells were washed once with PBS and incubated with biotin anti-CD140a (10 μg/ml; PDGFRα, clone APA5, BioLegend), APC anti-CD140b (10 μg/ml; PDGFRβ, clone APB5, BioLegend), Alexa Fluor 488 anti-BMPR1A (2 μg/ml; C32447, Signalway Antibody), Alexa Fluor 647 anti-BMPR1B (2 μg/ml; C32547, Signalway Antibody), Alexa Fluor 488 anti-BMPR2 (2 μg/ml; C32961, Signalway Antibody), or Alexa Fluor 647 anti-ACVR1 (2 μg/ml; C43627, Signalway Antibody). PE-streptavidin (1 μg/ml; BioLegend) was used with biotin anti-mouse CD140a. Cells were acquired on an LSR-Fortessa X-20 and analyzed with FlowJo software (TreeStar Inc.).

Binding of growth factors and IL-1β to ECM proteins

ELISA plates (Greiner Bio-One medium binding, Thermo Fisher Scientific) were coated with 100 nM ECM proteins in 50 μl of PBS for 1 hour at 37°C. Then, wells were washed with 400 μl of PBS-T (0.05% Tween 20) and blocked with 300 μl of BSA solution (1% in PBS-T) for 1 hour at room temperature. Wells without ECM protein coating and wells blocked only with the BSA solution were used as controls for nonspecific binding. ECM-coated wells and control wells were further incubated for 1 hour at room temperature with solutions murine PDGF-BB (PeproTech), IL-1Ra (R&D Systems), or $PlGF_{123–141}$-fused proteins at concentrations ranging from 0 to 100 nM (50 μl in PBS-T containing 0.1% BSA prepared in protein low-bind tubes (PROKEEP, Watson Bio Lab). Then, wells were washed three times with 300 μl of PBS-T and incubated for 1 hour with 50 μl of biotinylated polyclonal detection antibodies in PBS-T with 0.1% BSA. Detection antibodies used were PDGF-BB DuoSet ELISA (R&D Systems, DY8464) for PDGF-BB and IL-1ra/IL-1F3 DuoSet ELISA (R&D Systems, DY480) for IL-1Ra. Wells were further washed three times with PBS-T and incubated for 20 min with 50 μl of streptavidin–horseradish peroxidase (HRP). After three washes with PBS-T, 3,3',5,5'-tetramethylbenzidine (Thermo Fisher Scientific) was added followed by 50 μl of stop solution (0.16 M sulfuric acid). Concentrations of detection antibodies and streptavidin-HRP were used according to the manufacturer's instructions. To calculate the dissociation constants (K_d), specific-binding values were fitted with a one-site specific-binding model using absorbance at 450 nm (A_{450} nm) = Bmax × (growth factors or IL-1Ra variants)/[K_d + (growth factors or IL-1Ra variants)].

Release of growth factor and IL-1Ra variants from fibrin matrix

Fibrin matrices were generated with fibrinogen (8 mg/ml; Enzyme Research Laboratories), human thrombin (2 U/ml; Sigma-Aldrich), 5 mM $CaCl_2$, and growth factors (500 ng/ml) or IL-1Ra variants. Fibrin matrices were polymerized at 37°C for 1 hour and transferred to an Ultra-Low Cluster 24-well plate (Corning) containing 500 μl of buffer [20 mM tris-HCl, 150 mM NaCl, and 0.1% BSA (pH 7.4)]. Control wells that served as 100% released control contained only the growth factor and IL-1Ra variants in 500 μl of buffer. Every 24 hours, buffers were removed, kept at −20°C, and replaced with fresh buffer. For the 100% release control well, 20 μl of buffer was taken out every day and stored at −20°C. After 7 days, the cumulative release of growth factor and IL-1Ra variants was quantified by ELISA using the 100% released control as reference (BMP-2 DuoSet, PDGF-BB DuoSet, and IL-1Ra/IL-1F3 DuoSet; R&D Systems). For release assay with matrix metalloproteinases, the same method was used, except that the release buffer contained plasmin (100 μU/ml; Roche).

Recombinant growth factors and IL-1Ra variants

IL-1Ra/$PlGF_{123–141}$ and PDGF-BB/$PlGF_{123–141}$ were designed to bear a 6×His-tag at their N terminus and the $PlGF_{123–141}$ sequence at the C terminus. Recombinant proteins were produced in *Escherichia coli* via pET-22b (Novagen) and subsequently purified and refolded. Briefly, following protein production and bacterial lysis, the soluble fraction of IL-1Ra/$PlGF_{123–141}$ was purified by affinity chromatography using a chelating SFF(Ni) column with an extensive Triton X-114 wash [0.1% (v/v)] to remove endotoxins. PDGF-BB/$PlGF_{123–141}$ was extracted from inclusion bodies using a solubilization buffer [50 mM tris, 6 M GuHCl, and 10 mM dithiothreitol (pH 8.5)]. The extracted proteins were then added drop by drop in a refolding buffer [50 mM tris, 1 mM glutathione, and 0.1 mM oxidized glutathione (pH 8.2)] at 4°C, over 4 days, for a final protein solution to buffer ratio of 1:100. The refolded proteins were then purified by affinity chromatography using a chelating SFF(Ni) column with an extensive Triton X-114 wash [0.1% (v/v)] to remove endotoxins. The fraction containing dimers were pulled together. IL-1Ra/$PlGF_{123–141}$ was stored in PBS with 5 mM EDTA, while PDGF-BB/$PlGF\text{-}2_{123–141}$ was stored in 4 mM HCl. Murine wild-type IL-1Ra and BMP-2 were purchased from PeproTech and were endotoxin free.

Macrophage polarization

Calvarial defects were treated with fibrin matrices as described above. Matrices were functionalized with IL-1Ra IL-1Ra/$PlGF_{123–141}$ (250 ng). Mice were euthanized after 3, 6, 9, and 14 days after surgery, and matrices were harvested along with bone surrounding the defect area (1 mm farther). The harvested material was then mechanically broken down in smaller pieces and digested in collagenase XI (1 mg/ml; Gibco) at 37°C. After 30 min, 500 μl of serum was added, and the digested material was passed through a 70-μm cell strainer and centrifuged. Cells were washed in PBS and labeled with LIVE/DEAD Zombie Aqua (1:500 dilution; BioLegend) in PBS. Then, cells were washed once with PBS, and surface staining was performed for 15 min in PBS with 2% heat-inactivated FBS. Cells were fixed using FoxP3 fixation and permeabilization kit (eBioscience) and incubated with the following antibodies from BioLegend: anti-F4/80 FITC (clone BM8), anti-CD11b PE (clone M1/70), anti-CD80 BV421 (clone 16-10A1), and anti-CD206 PE-Cy7 (clone C068C2). Samples were acquired on

CyAn ADP (Beckman Coulter), and data were analyzed with FlowJo software (TreeStar Inc.).

Long bone defect

Mice (C57BL/6) used for surgery were 14 weeks old. Femoral defects and stabilization were made using the MouseFix plate 6-hole system, purchased from RISystem (RIS.401.130). In brief, mice were anesthetized with isoflurane. Their left hindlimb was shaved and scrubbed for aseptic surgery using iodine wipes. The skin and the fascia lata were incised from the hip joint to the knee, and the vastus lateralis and biceps femoris were split to expose the full length of the femur. The stabilization plate was fixed by four screws on the femur, and a 2-mm osteotomy was performed using a saw guide and wire saw. The defects were filled with a fibrin matrix polymerized between the restricted ends of the femur [40 µl per defect, fibrinogen (14 mg/ml; Enzyme Research Laboratories), thrombin (2 U/ml; Sigma-Aldrich), 5 mM $CaCl_2$, and aprotinin (25 µg/ml; Roche)]. The matrices were functionalized with 1 µg of BMP-2 and 1 µg of PDGF-BB/$PlGF_{123–141}$ with or without 1 µg of IL-1Ra/$PlGF_{123–141}$. Mice were euthanized 12 weeks after surgery, and femurs were analyzed by microCT.

Statistical analysis

All data are presented as means ± SEM. Statistical analyses were performed using GraphPad Prism 8 statistical software (GraphPad, USA). Significant differences were calculated with Student's *t* test or by analysis of variance (ANOVA), followed by the Bonferroni post hoc test when performing multiple comparisons between groups. $P < 0.05$ was considered as a statistically significant difference. The symbols *, **, and *** indicate *P* values less than 0.05, 0.01, and 0.001 respectively; n.s., not significant.

SUPPLEMENTARY MATERIALS

Supplementary material for this article is available at http://advances.sciencemag.org/cgi/content/full/6/24/eaba7602/DC1

View/request a protocol for this paper from *Bio-protocol*.

REFERENCES AND NOTES

1. X. Ren, M. Zhao, B. Lash, M. M. Martino, Z. Julier, Growth factor engineering strategies for regenerative medicine applications. *Front. Bioeng. Biotechnol.* **7**, 469 (2020).
2. M. M. Martino, P. S. Briquez, K. Maruyama, J. A. Hubbell, Extracellular matrix-inspired growth factor delivery systems for bone regeneration. *Adv. Drug Deliv. Rev.* **94**, 41–52 (2015).
3. P. S. Briquez, J. A. Hubbell, M. M. Martino, Extracellular matrix-inspired growth factor delivery systems for skin wound healing. *Adv. Wound Care (New Rochelle)* **4**, 479–489 (2015).
4. Y. Niu, Q. Li, Y. Ding, L. Dong, C. Wang, Engineered delivery strategies for enhanced control of growth factor activities in wound healing. *Adv. Drug Deliv. Rev.* **146**, 190–208 (2018).
5. Z. Julier, A. J. Park, P. S. Briquez, M. M. Martino, Promoting tissue regeneration by modulating the immune system. *Acta Biomater.* **53**, 13–28 (2017).
6. S. Naik, S. B. Larsen, C. J. Cowley, E. Fuchs, Two to tango: Dialog between immunity and stem cells in health and disease. *Cell* **175**, 908–920 (2018).
7. D. Wågsäter, C. Zhu, H. M. Björck, P. Eriksson, Effects of PDGF-C and PDGF-D on monocyte migration and MMP-2 and MMP-9 expression. *Atherosclerosis* **202**, 415–423 (2009).
8. E. Pardali, L.-M. Makowski, M. Leffers, A. Borgscheiper, J. Waltenberger, BMP-2 induces human mononuclear cell chemotaxis and adhesion and modulates monocyte-to-macrophage differentiation. *J. Cell. Mol. Med.* **22**, 5429–5438 (2018).
9. C. Garlanda, C. A. Dinarello, A. Mantovani, The interleukin-1 family: Back to the future. *Immunity* **39**, 1003–1018 (2013).
10. M. M. Martino, K. Maruyama, G. A. Kuhn, T. Satoh, O. Takeuchi, R. Müller, S. Akira, Inhibition of IL-1R1/MyD88 signalling promotes mesenchymal stem cell-driven tissue regeneration. *Nat. Commun.* **7**, 11051 (2016).
11. M. S. Rahman, N. Akhtar, H. M. Jamil, R. S. Banik, S. M. Asaduzzaman, TGF-β/BMP signaling and other molecular events: Regulation of osteoblastogenesis and bone formation. *Bone Res.* **3**, 15005 (2015).
12. Y. Zhang, C. Chang, D. J. Gehling, A. Hemmati-Brivanlou, R. Derynck, Regulation of Smad degradation and activity by Smurf2, an E3 ubiquitin ligase. *Proc. Natl. Acad. Sci. U.S.A.* **98**, 974–979 (2001).
13. T. Mund, M. J. Lewis, S. Maslen, H. R. Pelham, Peptide and small molecule inhibitors of HECT-type ubiquitin ligases. *Proc. Natl. Acad. Sci. U.S.A.* **111**, 16736–16741 (2014).
14. B. D. Manning, L. C. Cantley, AKT/PKB signaling: Navigating downstream. *Cell* **129**, 1261–1274 (2007).
15. E. Sierecki, W. Sinko, J. A. McCammon, A. C. Newton, Discovery of small molecule inhibitors of the PH domain leucine-rich repeat protein phosphatase (PHLPP) by chemical and virtual screening. *J. Med. Chem.* **53**, 6899–6911 (2010).
16. H. Zhang, S. N. Cohen, Smurf2 up-regulation activates telomere-dependent senescence. *Genes Dev.* **18**, 3028–3040 (2004).
17. Y. Kong, H. Cui, H. Zhang, Smurf2-mediated ubiquitination and degradation of Id1 regulates p16 expression during senescence. *Aging Cell* **10**, 1038–1046 (2011).
18. C. Ramkumar, Y. Kong, S. E. Trabucco, R. M. Gerstein, H. Zhang, Smurf2 regulates hematopoietic stem cell self-renewal and aging. *Aging Cell* **13**, 478–486 (2014).
19. F. Debacq-Chainiaux, J. D. Erusalimsky, J. Campisi, O. Toussaint, Protocols to detect senescence-associated beta-galactosidase (SA-βgal) activity, a biomarker of senescent cells in culture and in vivo. *Nat. Protoc.* **4**, 1798–1806 (2009).
20. J. E. Sims, D. E. Smith, The IL-1 family: Regulators of immunity. *Nat. Rev. Immunol.* **10**, 89–102 (2010).
21. M. M. Martino, P. S. Briquez, E. Güç, F. Tortelli, W. W. Kilarski, S. Metzger, J. J. Rice, G. A. Kuhn, R. Müller, M. A. Swartz, J. A. Hubbell, Growth factors engineered for super-affinity to the extracellular matrix enhance tissue healing. *Science* **343**, 885–888 (2014).
22. P. J. Murray, T. A. Wynn, Protective and pathogenic functions of macrophage subsets. *Nat. Rev. Immunol.* **11**, 723–737 (2011).
23. M. Manassero, V. Viateau, R. Matthys, M. Deschepper, R. Vallefuoco, M. Bensidhoum, H. Petite, A novel murine femoral segmental critical-sized defect model stabilized by plate osteosynthesis for bone tissue engineering purposes. *Tissue Eng. Part C Methods* **19**, 271–280 (2013).
24. P. S. Gomes, M. H. Fernandes, Rodent models in bone-related research: The relevance of calvarial defects in the assessment of bone regeneration strategies. *Lab. Anim* **45**, 14–24 (2011).
25. J. Chang, F. Liu, M. Lee, B. Wu, K. Ting, J. N. Zara, C. Soo, K. Al Hezaimi, W. Zou, X. Chen, D. J. Mooney, C.-Y. Wang, NF-κB inhibits osteogenic differentiation of mesenchymal stem cells by promoting β-catenin degradation. *Proc. Natl. Acad. Sci. U.S.A.* **110**, 9469–9474 (2013).
26. T.-H. Lin, E. Gibon, F. Loi, J. Pajarinen, L. A. Córdova, A. Nabeshima, L. Lu, Z. Yao, S. B. Goodman, Decreased osteogenesis in mesenchymal stem cells derived from the aged mouse is associated with enhanced NF-κB activity. *J. Orthop. Res.* **35**, 281–288 (2017).
27. E. W. Bradley, L. R. Carpio, M. E. McGee-Lawrence, C. Castillejo Becerra, D. F. Amanatullah, L. E. Ta, M. Otero, M. B. Goldring, S. Kakar, J. J. Westendorf, Phlpp1 facilitates post-traumatic osteoarthritis and is induced by inflammation and promoter demethylation in human osteoarthritis. *Osteoarthr. Cartil.* **24**, 1021–1028 (2016).
28. M. P. Baar, E. Perdiguero, P. Muñoz-Cánoves, P. L. de Keizer, Musculoskeletal senescence: A moving target ready to be eliminated. *Curr. Opin. Pharmacol.* **40**, 147–155 (2018).
29. A. M. Josephson, V. Bradaschia-Correa, S. Lee, K. Leclerc, K. S. Patel, E. Muinos Lopez, H. P. Litwa, S. S. Neibart, M. Kadiyala, M. Z. Wong, M. M. Mizrahi, N. L. Yim, A. J. Ramme, K. A. Egol, P. Leucht, Age-related inflammation triggers skeletal stem/progenitor cell dysfunction. *Proc. Natl. Acad. Sci. U.S.A.* **116**, 6995–7004 (2019).
30. A. Y. Simões Sato, G. L. Bub, A. H. Campos, BMP-2 and -4 produced by vascular smooth muscle cells from atherosclerotic lesions induce monocyte chemotaxis through direct BMPRII activation. *Atherosclerosis* **235**, 45–55 (2014).
31. A. Krettek, G. Ostergren-Lundén, G. Fager, C. Rosmond, G. Bondjers, F. Lustig, Expression of PDGF receptors and ligand-induced migration of partially differentiated human monocyte-derived macrophages. Influence of IFN-gamma and TGF-β. *Atherosclerosis* **156**, 267–275 (2001).
32. F. Wei, Y. Zhou, J. Wang, C. Liu, Y. Xiao, The immunomodulatory role of BMP-2 on macrophages to accelerate osteogenesis. *Tissue Eng. Part A* **24**, 584–594 (2018).
33. Z. Q. G. Liau, R. W. M. Lam, T. Hu, H.-K. Wong, Dose-dependent nerve inflammatory response to rhBMP-2 in a rodent spinal nerve model. *Spine (Phila Pa 1976)* **42**, E933–E938 (2017).
34. A. W. James, G. LaChaud, J. Shen, G. Asatrian, V. Nguyen, X. Zhang, K. Ting, C. Soo, A review of the clinical side effects of bone morphogenetic protein-2. *Tissue Eng. Part B Rev.* **22**, 284–297 (2016).

35. K.-B. Lee, C. E. Taghavi, S. S. Murray, K.-J. Song, G. Keorochana, J. C. Wang, BMP induced inflammation: A comparison of rhBMP-7 and rhBMP-2. *J. Orthop. Res.* **30**, 1985–1994 (2012).
36. E. S. Krell, C. W. DiGiovanni, The efficacy of platelet-derived growth factor as a bone-stimulating agent. *Foot Ankle Clin.* **21**, 763–770 (2016).
37. J. Ramírez, J. D. Cañete, Anakinra for the treatment of rheumatoid arthritis: A safety evaluation. *Expert Opin. Drug Saf.* **17**, 727–732 (2018).
38. M. M. Martino, F. Tortelli, M. Mochizuki, S. Traub, D. Ben-David, G. A. Kuhn, R. Müller, E. Livne, S. A. Eming, J. A. Hubbell, Engineering the growth factor microenvironment with fibronectin domains to promote wound and bone tissue healing. *Sci. Transl. Med.* **3**, 100ra189 (2011).
39. M. Kaipel, S. Schützenberger, A. Schultz, J. Ferguson, P. Slezak, T. J. Morton, M. Van Griensven, H. Redl, BMP-2 but not VEGF or PDGF in fibrin matrix supports bone healing in a delayed-union rat model. *J. Orthop. Res.* **30**, 1563–1569 (2012).
40. B.-B. Seo, J.-T. Koh, S.-C. Song, Tuning physical properties and BMP-2 release rates of injectable hydrogel systems for an optimal bone regeneration effect. *Biomaterials* **122**, 91–104 (2017).
41. Y. M. Kolambkar, K. M. Dupont, J. D. Boerckel, N. Huebsch, D. J. Mooney, D. W. Hutmacher, R. E. Guldberg, An alginate-based hybrid system for growth factor delivery in the functional repair of large bone defects. *Biomaterials* **32**, 65–74 (2011).
42. A. Shekaran, J. R. García, A. Y. Clark, T. E. Kavanaugh, A. S. Lin, R. E. Guldberg, A. J. García, Bone regeneration using an alpha 2 beta 1 integrin-specific hydrogel as a BMP-2 delivery vehicle. *Biomaterials* **35**, 5453–5461 (2014).
43. C. W. DiGiovanni, S. Lin, M. Pinzur, Recombinant human PDGF-BB in foot and ankle fusion. *Expert Rev. Med. Devices* **9**, 111–122 (2012).

Acknowledgments

Funding: This work was partially funded in part by the Swiss National Science Foundation (P2ELP3_175071) to Z.J., the Australian Research Council (DE170100398) to M.M.M., and the National Health and Medical Research Council (APP1140229 and APP1176213) to M.M.M. The Australian Regenerative Medicine Institute is supported by grants from the State Government of Victoria and the Australian Government. **Author contributions:** Z.J., R.K., B.N., Y.-Z.L., A.J.P., K.M., and M.M.M. conducted the experiments and analyzed the data. G.A.K. and R.M. contributed to microCT measurements and analyses. M.M.M. and Z.J. wrote the manuscript. M.M.M. and S.A. supervised the research. M.M.M. designed the research. **Competing interests:** M.M.M. is inventor on U.S. Patent 9,879,062, which covers one of the technologies reported in this article. Monash University has filed for patent protection on the molecular design described herein, and Z.J. and M.M.M. are named as inventors. The other authors declare that they have no competing interests. **Data and materials availability:** All data needed to evaluate the conclusions in the paper are present in the paper and/or the Supplementary Materials. Additional data related to this paper may be requested from the authors.

Submitted 2 January 2020
Accepted 29 April 2020
Published 12 June 2020
10.1126/sciadv.aba7602

Citation: Z. Julier, R. Karami, B. Nayer, Y.-Z. Lu, A. J. Park, K. Maruyama, G. A. Kuhn, R. Müller, S. Akira, M. M. Martino, Enhancing the regenerative effectiveness of growth factors by local inhibition of interleukin-1 receptor signaling. *Sci. Adv.* **6**, eaba7602 (2020).